



# On open boundary conditions for a limited-area coastal model off Oregon. Part 1: Response to idealized wind forcing

Jianping Gan<sup>\*</sup>, J.S. Allen

*College of Oceanic and Atmospheric Sciences, Oregon State University, Corvallis, OR 97331-5503, USA*

Received 16 September 2003; received in revised form 10 December 2003; accepted 10 December 2003

Available online 31 January 2004

---

## Abstract

A two-part study focusing on the development and application of open boundary conditions (OBCs) for a limited-area high-resolution coastal ocean model off Oregon is pursued. In Part 1, the OBCs are formulated and evaluated in numerical experiments utilizing idealized wind forcing. In Part 2, the OBCs are applied in an experiment with forcing by space and time variable winds obtained from a regional mesoscale atmospheric model. The initial experiments in Part 1 involve forcing by winds that are constant in time and are spatially uniform. The response to both upwelling favorable (southward) and downwelling favorable (northward) winds are examined and compared to results obtained with cyclic alongshore boundary conditions (CBCs). Additional experiments are conducted with idealized spatial variability in the wind forcing to include assessment of the OBC performance in situations when coastal trapped wave (CTW) dynamics play an important role in the shelf flow response. Some aspects of OBC performance with time-dependent wind forcing are investigated in these latter experiments by examining the response after wind forcing is turned off. The OBCs separate the total baroclinic solution at the open boundary into local and global components. In these applications, the local solution is obtained from an across-shore, depth and time-dependent two-dimensional submodel. The existence of inflow or outflow is determined from the global solutions using radiation conditions. During inflow, the local solution is smoothly imposed. During outflow, the global part of the solution is radiated out of the domain. Favorable, dynamically consistent performance of these OBCs is found in all experiments.

© 2004 Elsevier Ltd. All rights reserved.

*Keywords:* Open boundary conditions; Modeling; Coastal ocean circulation

---

---

<sup>\*</sup> Corresponding author. Present address: Department of Mathematics and Atmospheric, Marine and Coastal Environment (AMCE) program, Hong Kong University of Science and Technology, Kowloon, Hong Kong.

*E-mail address:* [magan@ust.hk](mailto:magan@ust.hk) (J. Gan).

## 1. Introduction

In a limited-area high-resolution coastal ocean model, open boundary conditions (OBCs) are typically required to solve the model equations. Informative studies of open boundary condition implementation in ocean models have been presented by Chapman (1985) and recently by Palma and Matano (2000). The OBCs should allow a consistent specification of physical properties at the interface between the interior and the exterior of the computational domain. In particular, disturbances generated inside the domain should be able to travel outward across the open boundaries (OBs) without spurious reflection that would contaminate the interior solution. A concept commonly utilized in many OBCs is a Sommerfeld radiation type condition (Orlanski, 1976) based on a local application of the wave equation

$$\phi_t + C\phi_N = 0, \quad (1)$$

where  $\phi$  is any of model dependent variables,  $C$  is the propagation speed of disturbances,  $t$  is time,  $N$  is the coordinate normal to the OBs and subscripts denote partial differentiation. The fundamental assumption of this radiation condition is that disturbances propagate across the OB with a wave speed  $C$  determined from the interior solution using (1). Difficulties in finding an effective propagation speed of disturbances in complex environments, however, often limit the success of the OBCs. Raymond and Kuo (1984), using a two-dimensional wave equation, derived an oblique horizontal radiation condition with phase velocity components both normal and tangential to the boundary. That condition has recently been applied in a regional model off the US west coast by Marchesiello et al. (2001). Without external forcing in (1), the conditions at the OB are solely determined from the model solutions immediately adjacent to the OB. In this case, the OBCs are referred to as passive OBCs.

OBCs derived from (1) are only valid without forcing at the boundary. To obtain realistic solutions in cases with forcing at the boundary, methods to correctly integrate the outer information into the limited-area domain are needed. OBCs with this capability are referred to as active OBCs. In some oceanographic problems this outer information can have a major impact on the evolution of the interior solution. For the case of wind forcing on the boundary, Roed and Smedstad (1984) suggested separating the solution into local and global parts close to the open boundary. The local solution can be provided in different ways, e.g., from a reduced-physics model in which OBCs are not required, from an outer model solution obtained on a larger computational domain usually with coarser grid resolution, or from measurements. The remaining component of the solution is the global part which can carry information from the interior towards the open boundary. A radiation OBC is imposed on the global solution only. In Roed and Smedstad (1984), this technique of separating local and global solutions in the OBCs is applied to the shallow water equations. Recently, Dinniman and Klinck (2003) have utilized this condition with the three-dimensional primitive equations, but have applied it only to the barotropic depth-averaged components of the model velocity. The principal outlined by Roed and Smedstad (1984), involving the separation of the solution at the boundary into local and global parts, can be interpreted, however, as applicable to all model variables, i.e. to both barotropic and baroclinic components. This principal can be applied, in particular, to a nesting procedure where three-dimensional information is available from the outer solution. The local solution at the OB should have an influence on the model interior only during the condition of inward propagation at

the OB. A method to help insure a smooth transition between inward and outward fluxes may be necessary to adjust the flow regime at the OB in complex oceanographic cases.

In order to simplify the set-up of a high-resolution limited coastal model and avoid the uncertainty in OBCs, cyclic boundary conditions (CBCs) in the alongshore direction are sometimes applied (e.g., Gan and Allen, 2002a,b). For a limited time integration of wind-forced shelf flow dominated by local flow topography interactions, the errors introduced by CBCs appear, based on model-data comparisons, to be reasonably small, particularly over the inner shelf (Gan and Allen, 2002b; Oke et al., 2002). The results obtained in a coastal model with CBCs during a limited time integration can be treated as a well-defined benchmark solution for evaluation of comparable solutions obtained with OBCs to help evaluate the performances of the OBCs. In this two-part study, newly developed OBCs are implemented in a three-dimensional model and applied to the Oregon coast. In Part 1, the OBCs are formulated and applied in numerical experiments utilizing idealized wind forcing. These experiments include cases with idealized spatial variability in the wind that causes coastal trapped wave (CTW) dynamics to play an important role in the shelf flow response. The results of these cases show the importance of representing the effects of the outer region through physically reasonable local solutions. In Part 2 (Gan et al., 2004) the OBCs are applied in an experiment with forcing by space and time variable winds obtained from a regional mesoscale atmospheric model.

The outline of Part 1 is as follows. The ocean model and its implementation are introduced in Section 2. The formulation of the OBCs is presented in Section 3. Comparisons of model results obtained with spatially uniform wind forcing using both CBCs and OBCs are given in Section 4. The response of the coastal model with OBCs in experiments with idealized spatial and temporal variability in the wind forcing is discussed in Section 5. A summary of the findings is given in Section 6.

## 2. The ocean model

The model used is the Princeton Ocean Model (POM) (Blumberg and Mellor, 1987) for three-dimensional, time-dependent oceanographic flows governed by the hydrostatic primitive equations. The Mellor and Yamada (1980) level 2.5 turbulent closure scheme is used to parameterize vertical mixing. The model domain extends alongshore 634 km from 41.7°N to about 47.3°N, and offshore 250 km with the coastline boundary fitted by a curvilinear coordinate (Fig. 1). The  $(x, y)$  horizontal curvilinear coordinates are positive in the eastward and northward directions, respectively. The across-shore and alongshore velocity components in the  $(x, y)$  directions are  $(u, v)$  with corresponding depth-averaged values designated by  $(U_A, V_A)$ . The surface elevation is  $\eta$ . The orientation of the offshore boundary has been rotated counterclockwise from north 0.2° so as to be better aligned with the coastline. Realistic continental shelf and bottom topography off Oregon is utilized. The model domain includes three open boundaries located on the north, south, and west, respectively. In order to include a directly comparable calculation using CBCs, regions with straight coastline of alongshore extent 10 km north of 47°N and 33 km south of 42°N are utilized. The shelf and slope topography is adjusted gradually so that it agrees at the north and south boundaries. Since the study is focused mainly on the flow field over the continental shelf, the maximum water depth is chosen to be 1200 m. The numbers of grid points in the alongshore,

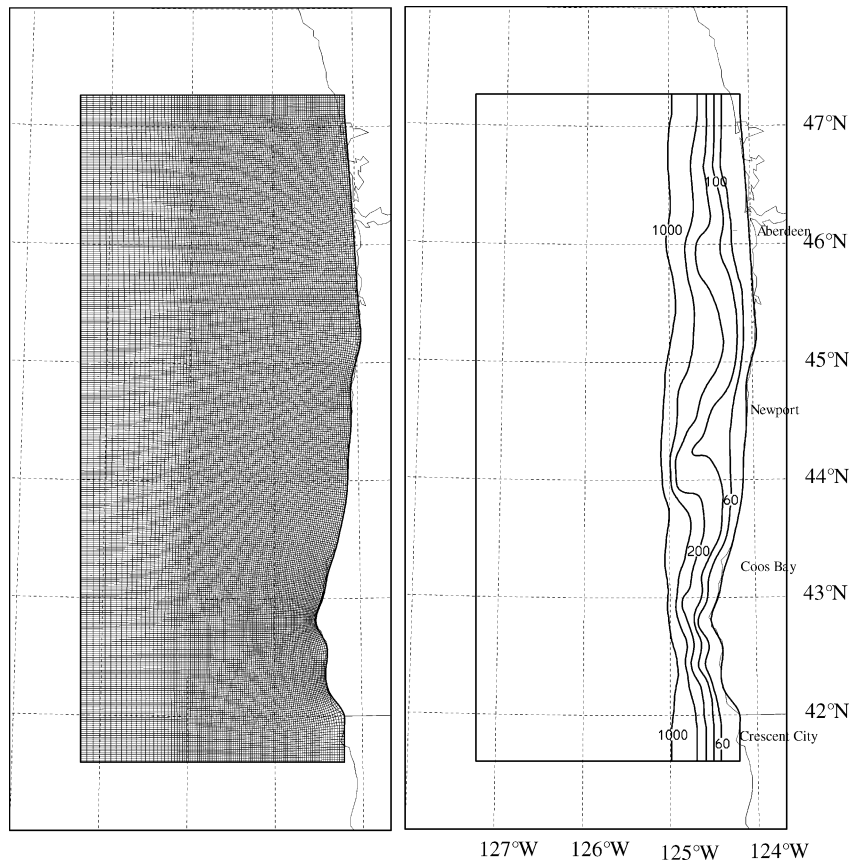


Fig. 1. Model curvilinear grid and bathymetry with the 60, 100, 200, 500 and 1000 m isobaths shown. The horizontal grid spacing ranges from 1.5 km near the coast to 6 km offshore with 45 vertical levels. The grid extends about 633 km alongshore and 250 km across-shore and contains three open boundaries.

across-shore and vertical ( $x, y, \sigma$ ) directions are (101, 327, 45). The horizontal grid spacing is variable, with minimum spacing near the coast ( $\Delta x = 1.5$  km,  $\Delta y = 1\text{--}2$  km) and a much larger grid size in  $x$  ( $\Delta x = 6$  km) in the western part of the domain.

The model is initialized with zero velocities and with horizontally uniform temperature and salinity profiles obtained from climatological values at a station 25 nautical miles off Newport. The space- and time-dependent structure of the wind stress forcing is varied in different experiments as described in Sections 4 and 5. Buoyancy flux from the atmosphere is set equal to zero for simplicity.

### 3. Formulation

For the CBCs, the model domain is represented by a channel that is periodic in the alongshore direction. The variables at the southern boundary (SB) and at the northern boundary (NB) (Fig. 1) are determined as follows.

$$\phi_{JM}^{n+1} = \phi_4^{n+1}, \quad \phi_{JM-1}^{n+1} = \phi_3^{n+1}, \quad \phi_2^{n+1} = \phi_{JM-2}^{n+1}, \quad \phi_1^{n+1} = \phi_{JM-3}^{n+1}, \quad (2)$$

where  $\phi$  represents all model dependent variables,  $n + 1$  is the forward time level, the grid points in  $y$  range from  $J = 1$  to  $J = JM$ , and the equations are solved from  $J = 3$  to  $J = JM - 2$ .

For passive OBCs, the phase speed of a disturbance (e.g., Chapman, 1985) is determined locally by,

$$C = \frac{\phi_{B\mp 1}^{n-1} - \phi_{B\mp 1}^{n+1}}{\phi_{B\mp 1}^{n+1} + \phi_{B\mp 1}^{n-1} - 2\phi_{B\mp 2}^n}, \quad (3)$$

where the subscript  $B$  stands for the grid point at the boundary,  $n$  is the current time level, and the upper and lower sign in  $\mp$  are for the right and left boundaries, respectively.

The solution at the OB is obtained following Camerlengo and O'Brien (1980) as:

if  $C < 0$  (inflow condition)

$$\phi_B^{n+1} = \phi_B^{n-1}, \quad (4)$$

if  $C > 0$  (outflow condition)

$$\phi_B^{n+1} = \phi_{B\mp 1}^n. \quad (5)$$

To incorporate the effects of forcing at the boundaries, active OBCs should be applied. For that case, the variables are divided into global and local parts following Roed and Smedstad (1984);

$$\phi = \phi_g + \phi_l. \quad (6)$$

In the numerical experiments discussed in this paper, the local solution  $\phi_l$  is obtained from simultaneous calculations utilizing local two-dimensional  $(x, \sigma, t)$  submodels at both the NB and SB. Since all of the alongshore  $y$  derivatives are set equal to zero in the two-dimensional submodel, the calculation of  $\phi_l$  is straightforward. To determine the relevant character of the boundary solution with regard to propagation directions, the local speed of a disturbance at the boundary is found from (3) using  $\phi_g$ , in which case  $C = C_{(g)}$ . Since the outer information influences the model solutions only during inflow condition, the solution at the OB is calculated separately for inflow and outflow conditions.

For inflow,  $C_{(g)} < 0$ ;

$$\phi_B^{n+1} = \phi_B^{n-1} - \frac{2\Delta t}{\lambda} [\phi_B^{n-1} - \phi_1^{n-1}]. \quad (7)$$

For outflow,  $C_{(g)} > 0$ ;

$$\phi_B^{n+1} = \phi_1^{n+1} + \phi_{gB}^{n+1}, \quad (8)$$

where

$$\phi_{gB}^{n+1} = \phi_{gB\mp 1}^n. \quad (9)$$

Here  $\phi$  represents  $(UA, u)$   $(VA, v)$ , potential temperature  $(\theta)$  and salinity  $(S)$ . The surface elevation  $\eta$  can also be treated in a similar manner although a no-gradient condition is chosen for  $\eta$  in this study, where  $\eta_B = \eta_{B\mp 1}$ . The parameter  $\lambda$  acts as a relaxation time scale in the inflow

conditions and is chosen to be 0.5 day. An examination of the sensitivity of the model solutions to  $\lambda$  is included in Section 5. In (7),  $\Delta t$  is the time step of the model integration and is equal to 140 s for the internal mode and 140/30 s for the external mode. The possibility of an increasing discrepancy between the two-dimensional solutions  $\phi_1$  at the open boundaries and the three-dimensional interior solutions near the boundary (see, e.g., the comparisons in Figs. 19 and 20 in Gan and Allen (2002a)), however, can limit the accuracy of model results for long time model integrations. An improvement in this procedure may be possible by providing external information from another model run in a larger domain using nesting. For that approach to be sensible, the outer model would itself have to have acceptable accuracy. To effectively reduce noisy fluctuations generated from radiation conditions, a weak spatial smoother is applied at every time step on the NB where outgoing coastal trapped waves exit. On the western boundary, UA is set to zero and the radiation condition of Camerlengo and O'Brien (1980) is utilized in VA,  $u$ , and  $v$ . A no-gradient condition is applied to  $\theta$  and  $S$ .

Mass conservation is enforced within the model domain for the experiments with OBCs. The net mass budget is calculated at each time step and a net influx or outflux, equally distributed in the across-boundary components of depth-averaged velocity along the three OBs, is imposed to conserve mass.

## **4. Response to spatially uniform wind forcing**

### *4.1. OBCs vs. CBCs*

In this section, solutions from the model with OBCs are compared with those obtained with CBCs to examine the effectiveness of the OBCs. Several experiments are run where first an idealized spatially uniform steady southward (upwelling) wind stress of magnitude 0.05 Pa is applied over the whole model domain. Second, a spatially uniform steady northward (downwelling) wind stress of the same magnitude is applied. The north and south directions referred to here are chosen to be parallel to the western boundary of the model (Fig. 1). We note that using a two-dimensional solution for the local part of the boundary solution (6) implies the assumption that the ocean behavior in the outer region is similar to that from an extended coast with no alongshore variations in topography or forcing. Cyclic boundary conditions, which have the important advantage of resulting in well-posed numerical problems with similar, manageable computational requirements, involve the assumption that the coastal topography and the forcing are periodic. Consequently, since these assumption differ, we should not expect exact agreement between the experiments with OBCs and CBCs. With the reasonably moderate topographic variations along the Oregon coast (Fig. 1) and with spatially uniform wind stress, however, we do anticipate useful comparisons of interior flow to help assess the OBC performance.

We run similar pairs of upwelling and downwelling experiments throughout this study because of differences in the coastal dynamics in these cases. Off Oregon, the direction of propagation of long coastal trapped waves (CTWs), e.g. Allen (1980), Brink (1991), is northward. Under southward (upwelling) wind stress the alongshore coastal currents are southward whereas for northward (downwelling) wind stress the currents are northward. This implies that for upwelling conditions, advection by the alongshore currents and propagation by CTWs are in opposite

directions. For downwelling, the advection and propagation directions are the same (northward). These dynamical factors can be expected to create challenges for the implementation of OBCs in different cases. To test the ability of the OBCs formulated here to handle different dynamical situations, we run both upwelling and downwelling experiments. In addition, in Section 5, we vary the spatial structure of the wind stress to check that the OBCs allow the correct behavior in situations where the shelf flow response is strongly influenced by CTW dynamics.

Fig. 2 shows the overall similarity in the fields of surface elevation and depth-integrated velocity from the solutions obtained with CBCs and OBCs after 15 days of integration in the upwelling case. Both solutions show the existence of a southward upwelling coastal jet over the shelf. They also show the offshore shifting of the jet and the formation of cyclonic circulation over Heceta

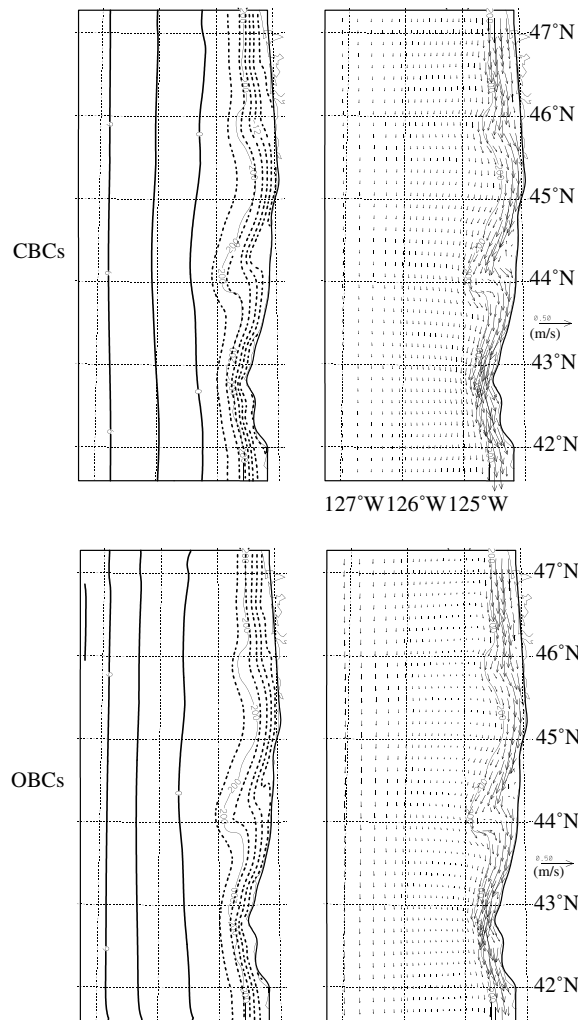


Fig. 2. Surface elevation (cm) and depth-averaged velocity vectors ( $\text{m s}^{-1}$ ) for the cases with CBCs and OBCs on day 15 during upwelling. Contour intervals for the surface elevation are 3 cm.

Bank between 44°N and 45°N. Slightly deeper depressions of surface elevation (about 3 cm) in the near coast region are found in the case with CBCs, reflecting a somewhat stronger coastal jet. Fields of both  $\eta$  and the velocity vectors obtained with OBCs show no evidence of reflection from either the northward propagation of long coastal trapped waves (CTWs) at the NB or from southward advection at the SB.

Across-shore ( $x, z$ ) sections of  $v$  at both the NB and the SB and at Newport (44.7°N) from both CBCs and OBCs are shown in Fig. 3. The presence of an alongshore upwelling coastal jet over the shelf and upper slope can be seen from south to north along the coast with both boundary conditions. The strength and the offshore location of the jet in the interior of the model domain at Newport are generally similar in both cases. The jet at the NB and SB, however, is stronger and located farther offshore in the case using CBCs with a larger difference at the NB. Consequently at Newport, the southward coastal jet and northward recirculation are also somewhat stronger. A possible physical explanation for the weaker currents at the NB and SB with OBCs is discussed below at the end of this subsection in connection with the behavior of the integrated transports across the boundaries.

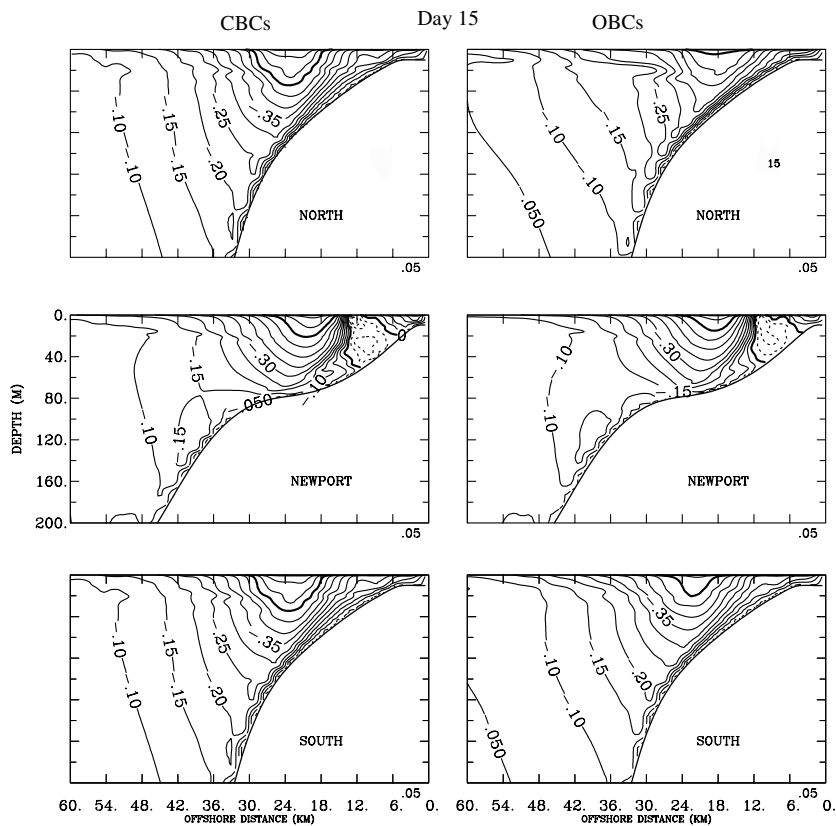


Fig. 3. Across-shore sections of daily averaged alongshore velocity  $v$  ( $\text{m s}^{-1}$ ) at the northern and southern boundaries and at Newport for the case forced with upwelling winds. Negative (positive) values of  $v$  are indicated by solid (dashed) contours. The contour interval for velocity is  $0.05 \text{ m s}^{-1}$  with heavy contour lines for  $-0.5 \text{ m s}^{-1}$ .

The across-shelf sections of  $v$  (Fig. 3) also illustrate the satisfactory behavior of the flow at the open boundaries and demonstrate the effectiveness of the OBCs in radiating waves and disturbances out of the model domain and in imposing reasonable outer advective fluxes. In particular, we have found that the application of a weak spatial smoother on the global part solutions on the NB where CTWs exit substantially reduces noisy fluctuations in the variables at that boundary.

For the case forced by downwelling favorable winds, the wind-driven coastal currents and CTWs both leave the model domain at the NB. No reflection is evident there in the  $\eta$  field or in the depth-averaged velocity field (Fig. 4). Compared to the upwelling case, the response of the wind-forced currents to variations in the bottom topography is weaker, with less across-shelf veering of the jet and no corresponding eddy formation over Heceta Bank (Figs. 2 and 3). The effects of Heceta Bank on the the coastal currents are qualitatively different during upwelling and

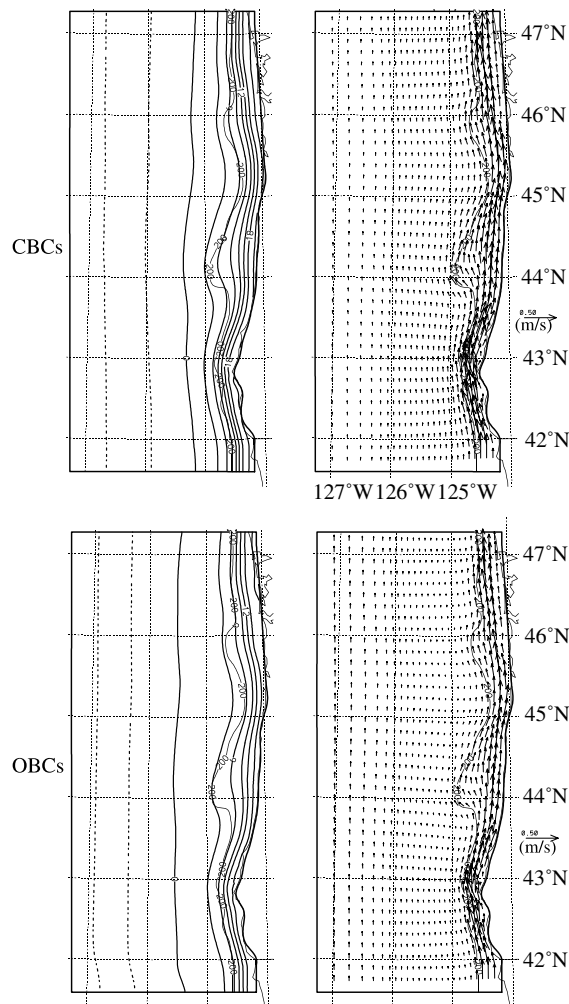


Fig. 4. Surface elevation (cm) and depth-averaged velocity vectors ( $\text{m s}^{-1}$ ) for the cases with CBCs and OBCs on day 15 during downwelling. Contour intervals for the surface elevation are 3 cm.

downwelling. Downwelling solutions from both CBCs and OBCs show very similar patterns in the depth-averaged  $v$  and in  $\eta$  which is elevated over the shelf. Similar to the results with upwelling winds, the alongshore coastal currents together with  $\partial\eta/\partial x$  have slightly larger magnitudes for the case with CBCs. The across-shore ( $x, z$ ) sections of  $v$  in Fig. 5 shows that  $v$  is about  $5 \text{ cm s}^{-1}$  larger at NB, SB and Newport from CBCs. The reasonable structure of the  $v$  sections at the NB and SB obtained with OBCs again illustrates satisfactory behavior of the flow at the boundaries in those experiments.

To see more clearly the manner in which the OBCs function we examine time series of  $x$  and  $z$  integrated alongshore transports across the NB and SB (Fig. 6). The transports are obtained by integrating  $v$  across-shore in  $x$  from the coast to 60 km offshore. We include the contributions from the local  $\text{Tr}_l$  and global  $\text{Tr}_g$  solutions, together with the total  $\text{Tr} = \text{Tr}_l + \text{Tr}_g$ .

Initially during the first 5 days, there is little contribution of  $\text{Tr}_g$  to the total transport and  $\text{Tr} \cong \text{Tr}_l$ , although there is a small deviation from this on the SB. For times after 5 days,  $\text{Tr}_g$  increases in magnitude slightly so as to reduce the relative magnitude of  $\text{Tr}$  compared to  $\text{Tr}_l$  in all cases. We believe that the reason for this is that shelf and slope topography variations in the interior of the domain support the set-up of alongshore pressure gradients which can geo-

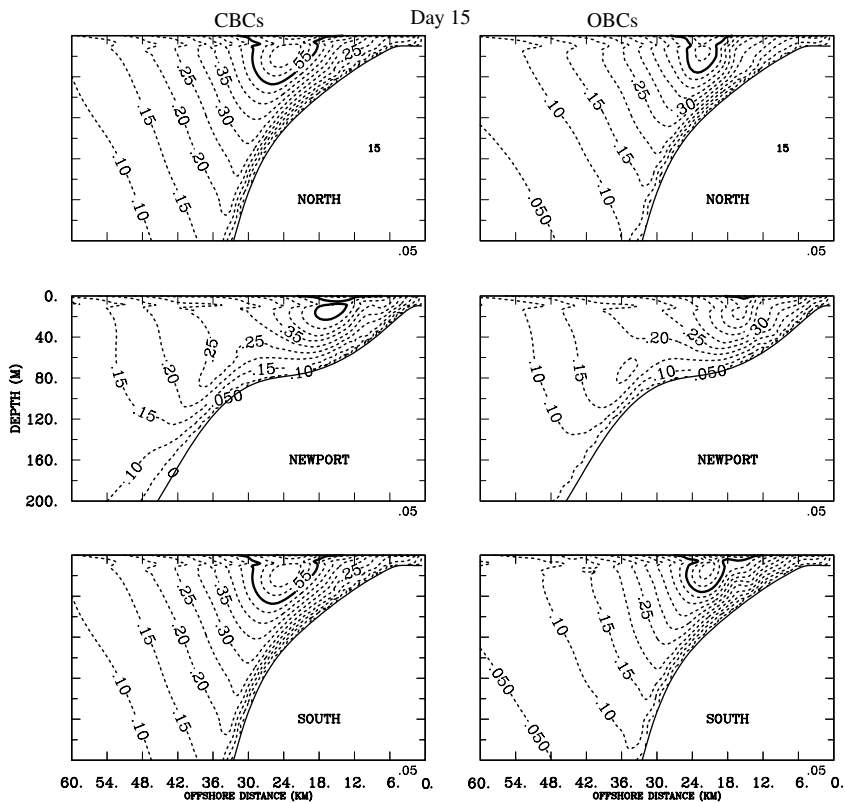


Fig. 5. Across-shore sections of daily averaged alongshore velocity  $v$  ( $\text{m s}^{-1}$ ) at the northern and southern boundaries and at Newport for the case forced with downwelling winds. Negative (positive) values of  $v$  are indicated by solid (dashed) contours. The contour interval for velocity is  $0.05 \text{ m s}^{-1}$  with heavy contour lines for  $0.5 \text{ m s}^{-1}$ .

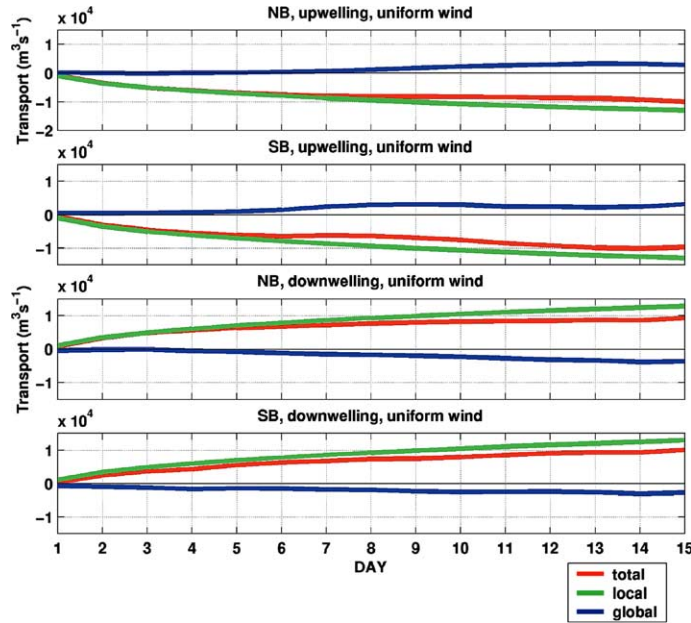


Fig. 6. Time series of daily averaged transports, from the coast to 60 km offshore, across the northern (NB) and southern (SB) boundaries for the experiments with spatially uniform winds during both upwelling and downwelling, respectively.

strophically balance the wind-forced across-shelf flow beneath the surface layer. This leads to a decrease in the acceleration of the alongshore coastal jet compared to the two-dimensional solutions utilized to find  $\phi_1$  and thus to  $|\text{Tr}| \leq |\text{Tr}_1|$ . Evidently, the behavior of the global part of the solutions at the boundary  $\phi_g$  is reflecting the adjustment of the boundary values to interior flow processes.

#### 4.2. Sensitivity to $\lambda$

As indicated in (7), the exact form of the OBCs depend on the value of the relaxation time scale  $\lambda$ . Two values of  $\lambda = 1$  day and  $\lambda = 0.25$  day, which are greater and less than basic case ( $\lambda = 0.5$  day), respectively, are utilized to examine the sensitivity of the solutions to the choice of  $\lambda$ . Some effects of changing  $\lambda$  can be seen clearly from  $v$  in the three across-shore sections at NB, SB and Newport (Figs. 7 and 8). Decreasing  $\lambda$  leads to an increase in the magnitude of  $v$  at all three sections for the upwelling case (Fig. 7). There is less sensitivity to  $\lambda$  evident in the  $v$  sections in the downwelling case (Fig. 8). Overall, the model solutions in these experiments do not appear to be overly sensitive to the exact choice of the value of  $\lambda$ . Ideally, the value of  $\lambda$  should be smaller than the time scale of the dominant physical process which for wind-driven coastal flows is in the order of 1–2 days. In experiments in Part 2 with realistic time variable winds (Gan et al., 2004), we have found, however, that a value of  $\lambda$  larger than 0.5 day is necessary to avoid nonphysical behavior, e.g. the appearance of large spatial gradient in the flow variables near the OBCs.

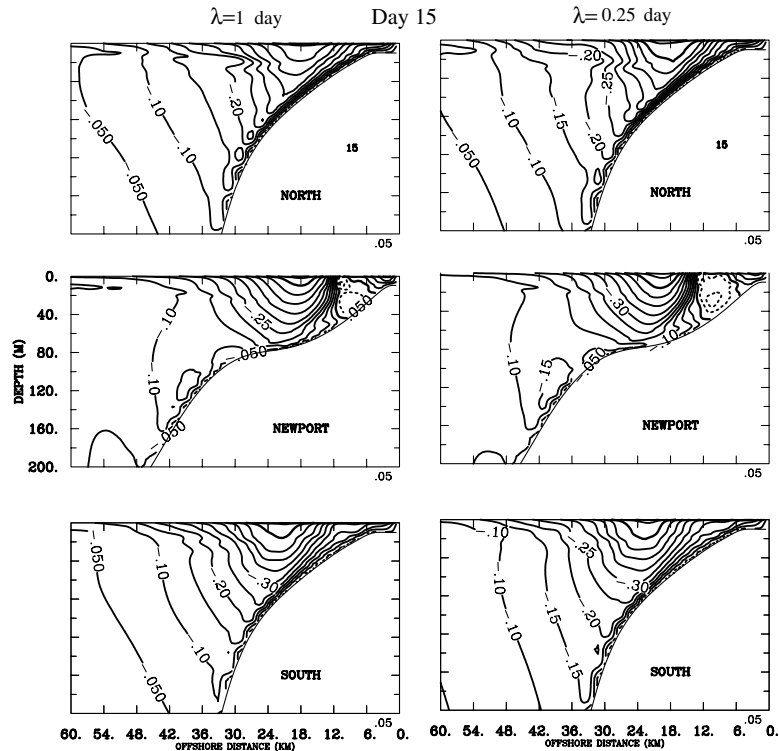


Fig. 7. Across-shore sections of daily averaged alongshore velocity  $v$  ( $\text{m s}^{-1}$ ) obtained with different values of  $\lambda$  at the locations of the northern and southern boundaries and at Newport during upwelling. Negative (positive) values of  $v$  are indicated by solid (dashed) contours. The contour interval for velocity is  $0.05 \text{ m s}^{-1}$  with heavy contour lines for  $-0.5 \text{ m s}^{-1}$ .

## 5. Response to spatially variable wind forcing

The results in Section 4 show promising performance of the OBCs in model solutions forced with spatially uniform winds. In reality, wind stress forcing is typically a function of both space and time. Along the Oregon coast in summer, the magnitude of the wind stress gradually increases in the southward direction and is up to a factor of 2–4 stronger south of the Cape Blanco ( $42.8^\circ\text{N}$ ) (Samelson et al., 2002). The desire to be able to include that spatial variability in the atmospheric forcing of Oregon coastal models, in fact, provided much of the motivation for the development of these OBCs. To examine the effectiveness of the OBCs under variable wind forcing, several different wind fields with idealized spatial and temporal variability are applied. In Part 2 (Gan et al., 2004), a realistic wind field obtained from a regional mesoscale atmospheric model (Samelson et al., 2002) is used to provide the forcing.

The imposition of spatially variable winds in the experiments here also has the advantage that it allows the ready assessment of the model and the OBC response in situations where CTWs play an important role. For the following discussion regarding expected CTW behavior, the idealized problem discussed in Allen (1976) provides a useful reference. In these experiments, the wind stress is again maintained as a constant in time for 15 days. Some aspects of the response to time

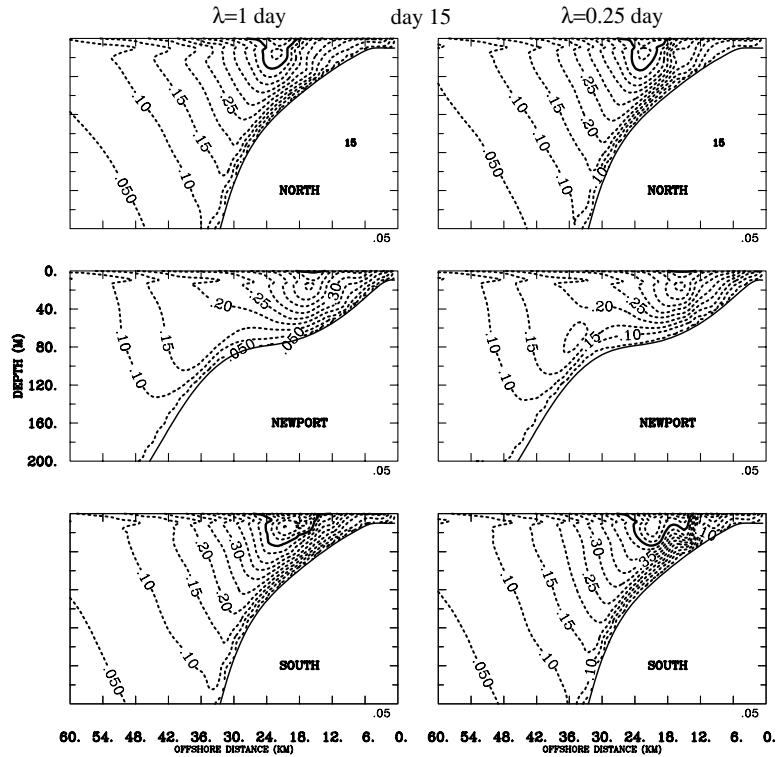


Fig. 8. Across-shore sections of daily averaged alongshore velocity  $v$  ( $\text{m s}^{-1}$ ) obtained with different values of  $\lambda$  at the locations of the northern and southern boundaries and at Newport during downwelling. Negative (positive) values of  $v$  are indicated by solid (dashed) contours. The contour interval for velocity is  $0.05 \text{ m s}^{-1}$  with heavy contour lines for  $0.5 \text{ m s}^{-1}$ .

variable winds are examined by subsequently setting the wind stress to zero after day 15. The time-dependent response during these parts of the experiments is discussed separately in Section 5.3.

### 5.1. No winds on the NB

In this experiment, the model is forced with a  $y$  dependent wind stress  $\tau(y)$  that has a magnitude of  $0.05 \text{ Pa}$  at the SB and that linearly decreases northward so that it zero at the NB. The wind stress  $\tau(y)$  is aligned in the north or the south direction as in Section 4. We use the notation  $\tau(y)$  to refer to a linear variation of  $\tau$  along the western boundary, such that the derivative  $\partial\tau/\partial y$  is a uniform constant over the entire domain. As in Section 4, model solutions forced with both upwelling and downwelling favorable  $\tau(y)$  are obtained. With  $\tau(y) = 0$  at the NB, the local solutions for velocities  $(u, v)$  in (7) and (8) are zero. The outgoing disturbances in the velocity components are only governed by the global solutions,  $\phi_g$  according to (8). At the SB, conditions similar to the uniform wind case can be expected. Alongshore gradients in the wind stress forcing field can be expected to excite CTWs, which subsequently propagate northward. Fig. 9 shows the progressive development in time in the offshore and northward directions of the shelf velocity field

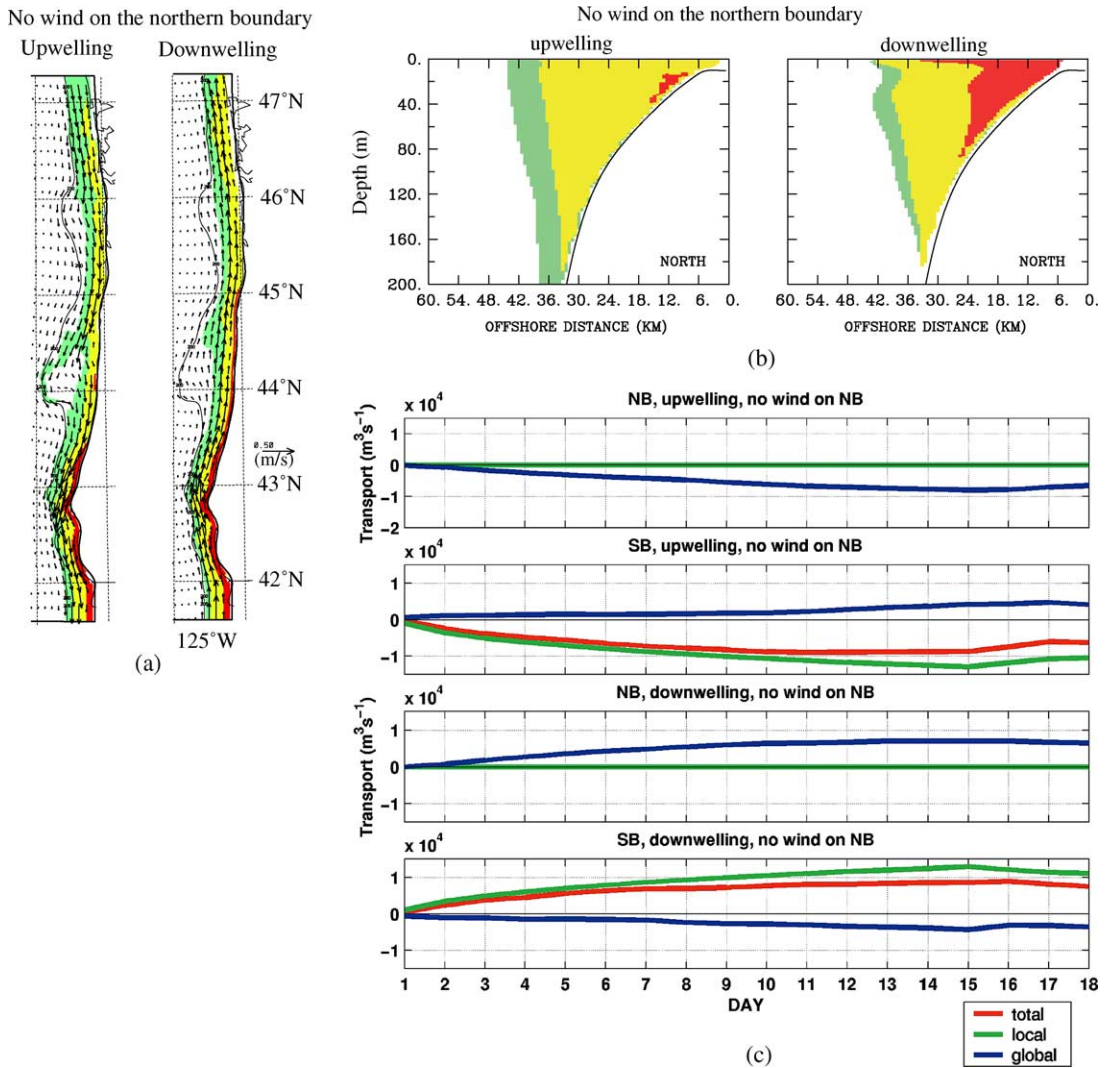


Fig. 9. (a) Magnitudes of the depth-averaged velocity with values greater than  $0.1 \text{ m s}^{-1}$  (color contours) on days 2 (red), 5 (yellow) and 10 (green) overlaid on the velocity vectors on day 15. (b) Across-shore sections of daily averaged alongshore velocities at the NB with values less/greater than  $-0.1/0.1 \text{ m s}^{-1}$  for upwelling/downwelling on days 5 (red), 10 (yellow) and 15 (green). (c) Time series of daily averaged transports, from the coast to 60 km offshore, across the northern (NB) and southern (SB) boundaries for the case with no wind at the NB during upwelling and downwelling, respectively. The winds are turned off after day 15.

as disturbances generated by the wind in the south propagate northward as CTWs. In both the upwelling and the downwelling favorable wind stress experiments, CTWs approach the NB by day 5 with a phase speed roughly estimated to be about  $1.6 \text{ m s}^{-1}$ . These waves appear to exit the domain cleanly without reflection. The arrival of CTWs at the NB can also be seen from sections of the alongshore velocity there at different times (Fig. 9b).

Time series of transports (Fig. 9c) at the NB show the expected zero contribution from  $Tr_1$  and the increase with time of southward (northward)  $Tr_g$  due to CTWs in the upwelling (downwelling) experiments. At the SB, the relative behavior of the transports is similar to that found in the spatially uniform wind experiment in Section 4.

### 5.2. No winds on the SB

In these experiments, the spatial distribution of both the upwelling and the downwelling favorable wind forcing  $\tau(y)$  is specified in a manner similar to that used Section 5.1, but with the magnitude of the wind stress decreasing linearly from 0.05 Pa at the NB to zero at the SB. Unlike the experiments in Section 5.1, the local solutions for the velocities are nonzero at the NB where CTWs exit the domain (Fig. 10a). With very weak wind stress in the southern part of the domain, CTWs are mainly excited in the northern region where they can quickly propagate northward out of the NB. Consequently, the alongshore velocity  $v$  is spun-up rapidly on the NB (Fig. 10b). The influence of CTWs on the development of coastal currents is much smaller than that found in the experiments in Section 5.1 in which CTWs are forced in the southern part of the domain and propagate northward along the entire coast. In the upwelling experiment, the directions of propagation of CTWs is opposite to that of the local velocity  $v_1$  at the NB. Whether (7) or (8) is utilized in this complex flow field is determined by the sign of phase speed determined from (3).

The behavior of the transports at the boundaries is shown in the time series plots in Fig. 10c. At the NB, the transport from the global solution  $Tr_g$  is opposite in sign to that in  $Tr_1$  and acts to reduce the magnitude of  $Tr$  relative to  $Tr_1$ . This can be explained as due to the adjustment through CTW propagation of the interior velocity field to near steady values, as pressure gradients develop to geostrophically balance wind-forced across-shore flow beneath the surface layer. The two-dimensional solutions used to find  $\phi_1$  do not include that adjustment mechanism and thus  $\phi_g$  must accomplish a compensation for that loss at the NB. It is notable that in the upwelling experiment the effects of southward advection remain weak in the southern part of the domain and have almost no effect on  $Tr$  at the SB.

### 5.3. Turning off winds

To test some aspects of the behavior of the OBCs with time-dependent wind stress, the  $\tau(y)$  applied in Section 5.1 (no wind at the NB) and in Section 5.2 (no wind at the SB) is turned off after day 15. The model is subsequently integrated for an additional 3 days through day 18 with no wind forcing.

For the case with no wind on the NB, the coastal currents retain the spatial structure present on day 15 with little decrease in magnitude after the winds are turned off (Fig. 11). This type of behavior is expected because the two-dimensional solution used to obtain  $v_1$  at the SB represents the effects of an outer coastal region of infinite alongshore extent. Thus, at the SB the cessation of the wind stress will only lead to slow changes of  $v_1$  with time due to the relatively weak effect of bottom friction (see, e.g., Fig. 20 in Gan and Allen (2002a)). This behavior may be seen for both upwelling and downwelling from the time variability of  $Tr_1$  at the SB during days 16–18 (Fig. 9c). As result, with only small changes in  $v_1$  at the SB, no appreciable variations in the shelf velocity field are caused by the effects of CTW propagation.

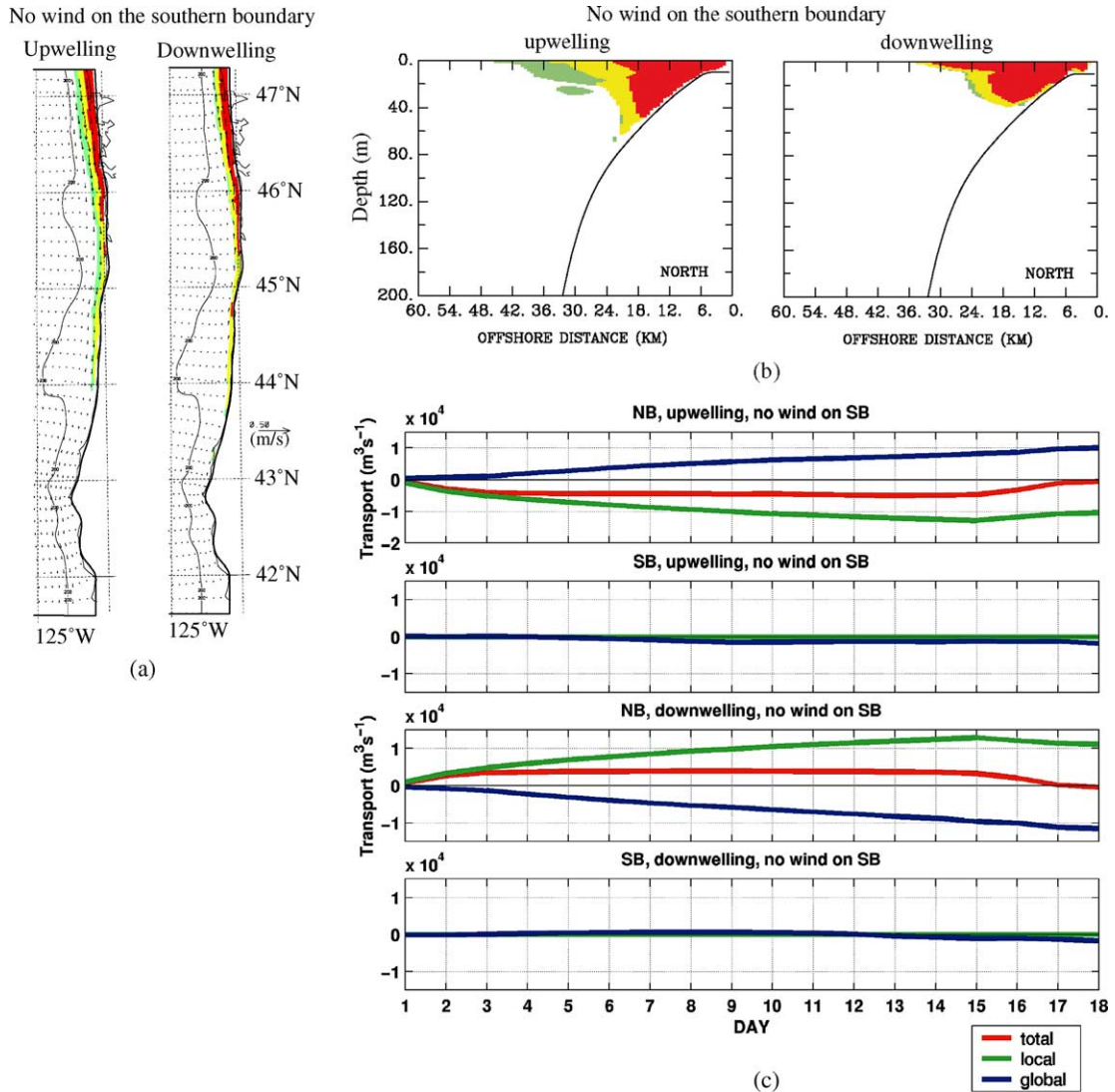


Fig. 10. (a) Same as Fig. 9a, but for the case with no wind on the SB. (b,c) Same as Fig. 9b and c, but with no winds on the SB.

In contrast, a qualitatively different response is found in the case with no wind on the SB (Fig. 12). The coastal currents quickly decrease in magnitude in the whole domain when the winds are turned off. This is due to the northward propagation in the form of CTWs of the  $y$ -dependent current fluctuations present on day 15. The OBCs (7) and (8) evidently allow these CTW disturbances to propagate out of the domain, as they should. This is in spite of the fact that at the NB  $v_1$  remains close to its day 15 values. Thus, the global solution  $v_g$  must be behaving in such a manner that the OBCs (7) and (8) correctly let CTW disturbances propagate northward out of the domain. This behavior is shown in the time series plots of transport in Fig. 10c where at the NB during days 16–18  $Tr_g$  nearly balances  $Tr_1$  and the magnitude of  $Tr$  decreases. By day 18,  $Tr$

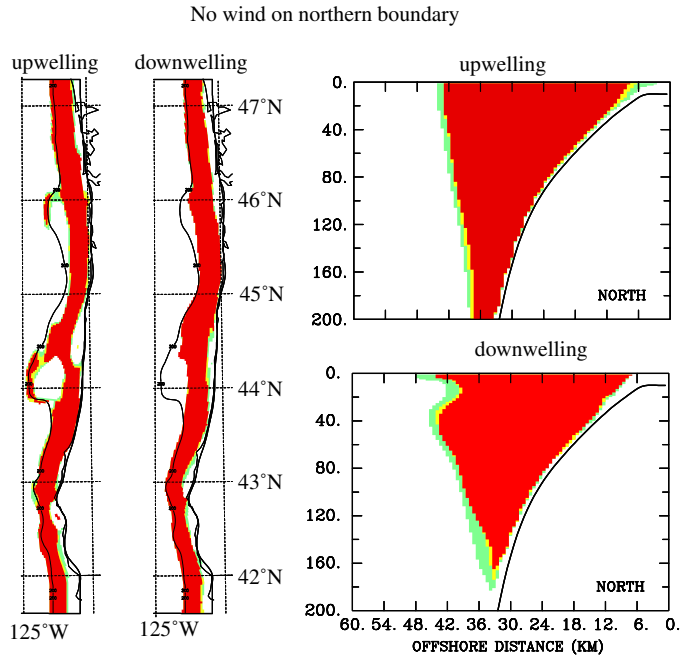


Fig. 11. (Left) Magnitudes of the depth-averaged velocity with values less/greater than  $-0.1/0.1 \text{ m s}^{-1}$  for upwelling/downwelling, respectively, on days 1, 2 and 3 (green, yellow and red) after the winds are turned off following day 15. (Right) The corresponding across-shore sections of daily average alongshore velocity at the NB with values less/greater  $-0.1/0.1 \text{ m s}^{-1}$  on days 1, 2 and 3 (green, yellow and red) are also shown.

reached very small values due to the generation of weak currents at depth, not evident in the section in Fig. 12, with direction opposite to the near surface coastal jet. In the present experiment with no wind on the SB,  $v_1$  remains equal to zero at the SB so that there is no source of energy for CTW disturbances from the south.

## 6. Summary

Open boundary conditions (OBCs) are developed and applied to a three dimensional, limited-area high-resolution coastal ocean model off Oregon. Initial experiments involve testing the OBCs in situations with idealized wind forcing. The inclusion of spatial variability in the winds allows the assessment of OBC performance in cases where CTW dynamics plays an important role in the coastal ocean response. To our knowledge, this is the first test of OBC functioning with regard to the behavior of wind-forced CTWs in a well resolved coastal model using the primitive equations with realistic three-dimensional shelf topography and realistic stratification.

The OBCs involve the separation of the full baroclinic solution at the boundary into global and local parts. In these experiments the local solution is obtained from a two-dimensional  $(x, \sigma, t)$  sub-model. The global solution is utilized to determine inflow or outflow conditions, based on an Orlandi (1976) radiation condition. During inflow, the local solution is smoothly imposed as a boundary

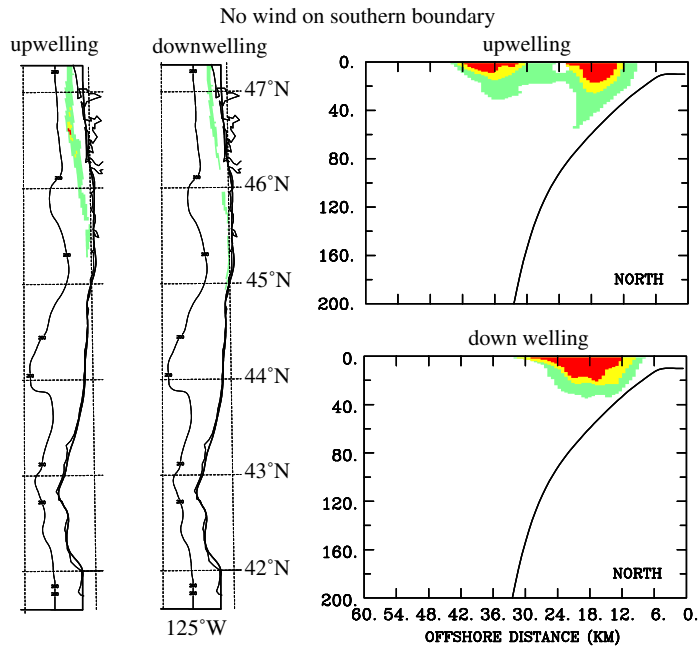


Fig. 12. Same as Fig. 11, but for the case with no wind on the SB.

condition. During outflow, the global solution is radiated out of the domain. In the experiments forced with spatially uniform winds, the OBCs give solutions that are reassuringly similar to those obtained with CBCs. In particular, the detailed structure of the solution at the OBs is physically reasonable. In the experiments forced with spatially variable winds, the OBCs give solutions that have behavior totally consistent with that expected from a consideration of CTW dynamics.

In general, the OBCs presented here are found to perform satisfactorily in numerical experiments with idealized wind forcing. These experiments are designed to isolate and test different physical aspects associated with the coastal ocean response. The application of these OBCs in a realistic simulation with time- and space-dependent wind forcing obtained from a regional mesoscale atmospheric model is discussed in Part 2 (Gan et al., 2004).

## Acknowledgements

This research was supported by the National Science Foundation Coastal Ocean Processes (CoOP) program under grant OCE-9907854. We thank two anonymous reviewers for helpful comments. J. Gan is grateful to Hong Kong University of Science and Technology for additional support.

## References

- Allen, J.S., 1976. Some aspects of the forced wave response of stratified coastal region. *J. Phys. Oceanogr.* 6, 113–119.
- Allen, J.S., 1980. Models of wind-driven currents on the continental shelf. *Ann. Rev. Fluid Mech.* 12, 389–433.

- Blumberg, A.F., Mellor, G.L., 1987. A description of a three-dimensional coastal ocean circulation model. In: Heap, N. (Ed.), *Three-Dimensional Coastal Ocean Models*, vol. 4. AGU, Washington, DC. pp. 208.
- Brink, K.H., 1991. Coastal-trapped waves and wind-driven currents over the continental shelf. *Ann. Rev. Fluid Mech.* 23, 389–412.
- Camerlengo, A.L., O'Brien, J.J., 1980. Open boundary condition in rotating fluids. *J. Comput. Phys.* 35, 12–35.
- Chapman, D.C., 1985. Numerical treatment of across-shore open boundaries in a barotropic ocean model. *J. Phys. Oceanogr.* 15, 1060–1075.
- Dinniman, M.S., Klinck, J.M., 2003. The influence of open versus periodic alongshore boundaries on circulation near submarine canyons. *J. Atmos. Technol.* 19, 1722–1737.
- Gan, J.P., Allen, J.S., 2002a. A modeling study of shelf circulation off northern California in the region of the Coastal Ocean Dynamics Experiment, Response to relaxation of upwelling winds. *J. Geophys. Res.* 107 (C9), 3123. Available from <doi:10.1029/2000JC000768>.
- Gan, J.P., Allen, J.S., 2002b. A modeling study of shelf circulation off northern California in the region of the Coastal Ocean Dynamics Experiment. 2. Simulations and comparisons with observations. *J. Geophys. Res.* 107 (C11), 3184. Available from <doi:10.1029/2001JC001190>.
- Gan, J.P., Allen, J.S., Samelson, R.M., 2004. On open boundary conditions for a limited-area coastal model off Oregon. Part 2: Response to wind forcing from a regional mesoscale atmospheric model. *Ocean Modell.*, this issue.
- Marchesiello, P., McWilliams, J.C., Schepetkin, 2001. Open boundary condition for long-term integration of regional oceanic models. *Ocean Modell.* 3, 1–20.
- Mellor, G.L., Yamada, T., 1980. Development of a turbulence closure model for geophysical fluid problems. *Rev. Geophys.* 20, 851–875.
- Oke, P.R., Allen, J.S., Miller, R.N., Egbert, G.D., Austin, J.A., Barth, J.A., Boyd, T.J., Kosro, P.M., Levine, M.D., 2002. A modeling study of the three-dimensional continental shelf circulation off Oregon. I. Model-data comparisons. *J. Phys. Oceanogr.* 32, 1360–1382.
- Orlanski, I., 1976. A simple boundary condition for unbounded hyperbolic flows. *J. Comput. Phys.* 21, 251–269.
- Palma, E.D., Matano, R.P., 2000. On the implementation of open boundary conditions for a general circulation model: The three-dimensional case. *J. Geophys. Res.* 105, 8605–8627.
- Raymond, W.H., Kuo, H.L., 1984. A radiation boundary condition for multidimensional flows. *Quart. J.R. Meteorol. Soc.* 110, 535–551.
- Roed, L.P., Smedstad, O.M., 1984. Open boundary conditions for forced waves in a rotating fluid. *SIAM J. Sci. Stat. Comput.* 5, 414–426.
- Samelson, R.M., Barbour, P., Barth, J., Bielli, S., Boyd, T., Chelton, D., Kosro, P., Levine, M., Skillingstad, E., Wilczak, J., 2002. Wind stress forcing of the Oregon coastal ocean during the 1999 upwelling season. *J. Geophys. Res.—Oceans* 107 (C5). Available from <doi:10.1029/2001JC000900>.